Article

Computational Insights into the Regioselectivity of 1,3-Dipolar Cycloadditions inside Carbon Nanotubes

Published as part of The Journal of Physical Chemistry C special issue "Francesc Illas and Gianfranco Pacchioni Festschrift".

Michele Tomasini, Tainah Dorina Marforio, Matteo Calvaresi,* Albert Poater,* and Jordi Poater*

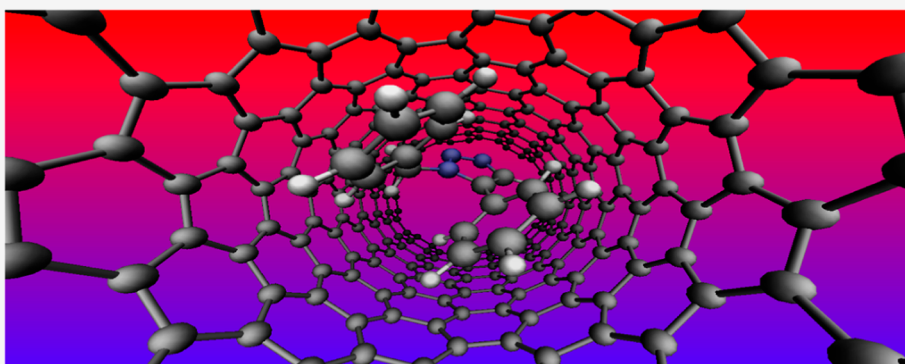Cite This: *J. Phys. Chem. C* 2024, 128, 14961–14971

Read Online

ACCESS | Metrics & More | Article Recommendations | SI Supporting Information

ABSTRACT: Nature's enzymes exhibit remarkable substrate specificity and catalytic efficiency by transforming substrates within confined active sites. To emulate this, various molecular containers, including zeolites, cyclodextrins, calix[n]arenes, cavitands, cucurbit[n]urils, metal–organic frameworks, covalent organic frameworks, and carbon nanotubes (CNTs), have been explored. Among these, CNTs are notable for their unique physical and chemical properties, enabling them to control reactions through spatial confinement. This study investigates the effect of CNT encapsulation on metal-free 1,3-dipolar Huisgen cycloaddition reactions between benzyl azide and substituted alkynes. Experimental results showed that CNTs significantly enhance the selectivity for the 1,4-triazole product. Computational studies using density functional theory further elucidate the impact of CNT confinement on reaction mechanisms and regioselectivity. The findings reveal that confinement within CNTs alters potential energy surfaces, favoring 1,4-triazole formation over 1,5-triazole, driven by steric and electronic factors. Additionally, comparative analyses highlight the influence of CNT diameter on activation energies and product stability, particularly with energy decomposition analysis and noncovalent interaction plots. This research underscores the potential of CNTs as nanoscale reactors for controlled synthesis, providing insights into the design of new catalytic systems and advancing the field of molecular encapsulation for selective organic transformations.

INTRODUCTION

Nature has developed enzymes to recognize specific substrates and transform them inside well-defined pockets that ensure product selectivity and enhance reaction rates.[1,2] To mimic nature, there is currently a wide selection of potential candidates, including zeolites,[3,4] cyclodextrins,[5,6] calix[n]-arenes,[7,8] cavitands,[9–11] cucurbit[n]urils,[12,13] and more recently, even metal–organic frameworks and covalent organic frameworks, despite their less potential.[14,15] All of them have been exploited or designed to control, through the encapsulation of guest molecules inside their cavities, kinetics and thermodynamics of a large number of chemical transformations.[16] The cavity environment is capable of altering the potential energy surface (PES) of the reaction, affecting kinetics and selectivity, and promoting spatial confinement as a

valuable methodology for controlling organic reactivity.[17] Actually, another class of molecular containers are carbon nanotubes (CNTs),[18,19] which can be seen as hollow nanocylinders, generated by rolling a graphene sheet.[20,21] The peculiar physical and chemical properties of CNTs can be exploited to govern confined reactions.[22] In addition, depending on the diameter of the CNT,[23] different-sized molecules
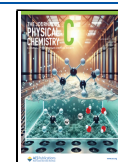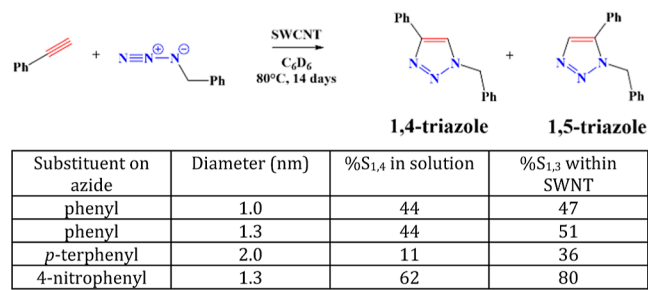
can be encapsulated,[24−27] allowing the desired molecules to be selectively trapped,[28] forming the bulk phase. Studies on metal-based catalytic reactions inside CNTs are mainly reported in the literature,[29−31] but only a limited number of metal-free CNT encapsulated reactions have been investigated.[32,33] The discovery of unique oligomers and polymers,[34] graphene,[35−37] inorganic nanoribbons,[38] nanotubes,[39,40] and molecular nano-diamonds[41] encapsulated within CNTs highlights the potential of narrow nanotubes as nanoscale reaction vessels.[42] These tubes control the formation of one-dimensional macro-molecular products that are difficult to produce by using other methods. However, strong interactions between the nanotube host and guest nanostructures prevent the extraction and characterization of the products, hindering preparative synthesis due to the product inhibition effect.

Recently, Rance and co-workers[43] investigated the effect of encapsulating metal-free 1,3-dipolar Huisgen cycloaddition reactions[44,45] described in narrow CNTs,[46] by performing the reaction between benzyl azide (1,3-dipole) and substituted alkynes (dipolarophiles). From a mechanistic point of view, the 1,3-dipolar cycloadditions are pericyclic reactions, where the 2π electrons of the dipolarophile and the 4π electrons of the 1,3-dipole generate a six-electron 5-membered-ring transition state (TS) in an aromatic patterned structure.[47] These reactions occur in the bulk phase at high temperatures and generate a mixture of regioisomers (1,4 and 1,5-triazoles), see Scheme 1. For instance, to prove the effect of increasing the

Scheme 1. Huisgen Reaction with/without CNTs

		1,4-triazole	1,5-triazole
Substituent on azide	Diameter (nm)	%$S_{1,4}$ in solution	%$S_{1,3}$ within SWNT
phenyl	1.0	44	47
phenyl	1.3	44	51
p-terphenyl	2.0	11	36
4-nitrophenyl	1.3	62	80

steric bulk of the alkyne reactant, in the case of *p*-terphenyl, $S_{1,4}$ regioselectivity increased upon 11% inside the nanotube, or, with the aim to test the effect of the electronic effects, 4-nitrophenyl, also enclosed in Scheme 1, increased the $S_{1,4}$ regioselectivity up to 18%. Thus, in general, the presence of CNT enhances the selectivity for the 1,4-triazole product by up to 55% with respect to the bulk phase (benzene).[46] To explain this experimental evidence, the authors suggested that product geometry, steric effects, and polarizability of the CNT are responsible for the increased regioselectivity inside the CNT. In extreme cases, the most significant increase in $S_{1,4}$ regioselectivity upon confinement was noted for the alkyne featuring the most electron-withdrawing *para*-substituent, particularly exemplified by 4-nitrophenylacetylene. Conversely, the opposite trend was observed for *p*-terphenyl. This study was nearly revolutionary since it was the second apart from the former organic chemical reaction carried out experimentally inside narrow CNTs without the aid of a catalyst: the aromatic halogenation reaction.[48] This reaction demonstrated that the intense spatial constraints within narrow single-walled CNTs (SWCNTs) guided the site-selective electrophilic attack of the confined aromatic guest reactant. Consequently, there was a

significant increase in the formation of the preferred linear *para*-regioisomer, with the yield rising to an impressive 97%. This observation underscored the remarkable influence of nanotube confinement on reaction outcomes, offering intriguing possibilities for controlled synthesis within nanoscale environments. Next, computational studies complemented the understanding of confining reactions inside several types of CNTs. In particular, apart from a descriptive work,[49] specially by Yumura et al.,[50−52] the reactivity was unveiled inside CNTs,[52−56] like the general Diels−Alder[57] and S_N2 reactions,[58−61] or the rather specific aromatic bromination of *N*-phenylacetamide inside CNTs.[62] In particular, Fukuura and Yumura conducted density functional theory (DFT) calculations to analyze 1,3-dipolar cycloadditions involving phenyl-acetylene and phenylazide or benzylazide within CNTs with diameters ranging from 10 to 14 Å. The study focused on optimizing the structures of reaction species, constructing PESs in terms of the reaction pathway. Key parameters such as activation energy and stability of the products were determined to understand the regioselectivity of these cycloadditions. Comparative analysis with gas-phase reactions was undertaken to discern the impact of nanotube confinement on the regioselectivity modulation. Results revealed that nanotube confinement significantly favors the formation of 1,4-triazoles over 1,5-triazoles, enhancing both kinetic and thermodynamic control. Performed energy decomposition analyses also identified two main factors affecting regioselectivity: destabi-lization of the reactant complex (RC) in 1,4-approaches and increased activation energies in 1,5-approaches due to phenyl overlapping styles dictated by tube diameter. In thin tubes, repulsive orbital interactions between phenyl rings in 1,5-approaches led to higher activation energies, favoring 1,4-triazole formation. Conversely, in both 1,4 and 1,5-approaches, the stability of products was less affected by phenyl interactions due to their stacking configuration. Thus, nanotube confine-ment selectively modulates PESs to promote the formation of 1,4-triazoles, elucidating the role of nanotubes in controlling regioselectivity in 1,3-dipolar cycloadditions.[63]

In the present paper, we aim to further clarify, by means of computational methods, the factors that govern the regiose-lectivity inside the CNT for the 1,3-dipolar cycloaddition reactions studied by Rance and co-workers.[43] We used either a full DFT approach to study the reactions in the bulk phase (benzene) or a hybrid QM/MM approach to investigate encapsulated reactions. The hybrid methodology was reported to reliably describe CNT confined reactions,[62] and the results may lead to future predictions.[64,65]

■ COMPUTATIONAL DETAILS

All DFT calculations were performed using the Gaussian16 package.[66] Geometry optimizations utilized the B97 functional, a hybrid GGA functional originally developed by Becke[67,68] and then by Head-Gordon and Chai,[69] along with the Grimme D3 dispersion correction.[70] The calculations involved the all-electron 6-311 + G(d,p) basis set.[71,72] Symmetry constraints were not applied during the optimizations, and the nature of the stationary points was confirmed through an analytical frequency analysis. The QM/MM calculations[73] were con-ducted with the electronic embedding and Qeq formalism. Gibbs free energies at 353.15 K were computed using the B97-D3 functional[74] and the triple-ζ basis set 6-311 + G(d,p) for all atoms.[75] Solvent effects were considered using the universal solvation model PCM,[76−78] with benzene as the solvent. The

reported Gibbs free energies include electronic energies obtained at the B97-D3/6-311+G(d,p)(PCM(benzene))// B97-D3/6-311+G(d,p) level of theory. These values were corrected for zero-point vibrational energies, thermal corrections, and entropy effects computed at the B97-D3/6-311+G(d,p) level. The nanotube models are limited to 24 Å long, as in our previous analyses.[62] Moreover, the atoms of the nanotube are allowed to relax during geometry optimization. The choice of functional[79−81] and basis set[65,82] is validated by previous studies on carbon nanostructures.

A quantitative Kohn−Sham molecular orbital theory in combination with a quantitative energy decomposition analysis (EDA) in the gas phase has been performed with the Amsterdam density functional program.[83−85] For such, the dispersion-corrected DFT at the ZORA-BLYP-D3(BJ)/TZP level of theory has been used. The interaction energy ΔE_{int} between these fragments is decomposed into the classical electrostatic attraction ΔV_{elstat}, Pauli repulsion ΔE_{Pauli} between occupied orbitals, stabilizing orbital interactions ΔE_{oi}, and dispersion ΔE_{disp}. The strain energy is the energy difference between the fully relaxed geometry and that adopted by the fragments in the interacting system. Atomic charges were computed with the Voronoi deformation density (Voronoi deformation density) method.[86,87]

RESULTS AND DISCUSSION

The 1,3-dipolar cycloaddition of benzyl azide to alkynes, also known as the Huisgen reaction, has been investigated through DFT calculations in benzene. The model systems under investigation are formed by the benzyl azide (1,3-dipole) and the substituted dipolarophiles enclosed in Scheme 2: (i) 4-nitrophenyl acetylene (system **1**), (ii) 4-bromophenyl acetylene (system **2**), (iii) phenyl acetylene (system **3**), (iv) 4-methoxyphenyl acetylene (system **4**), (v) 4-aminophenyl

Scheme 2. CNTs and Systems 1−6

(8,8) Armchair   (10,10) Armchair

1   **2**   **3**

4   **5**   **6**
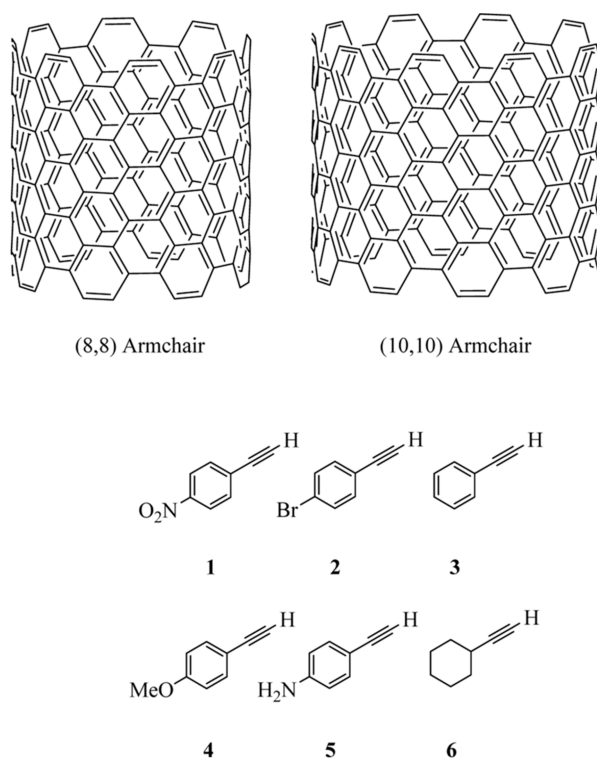
acetylene (system **5**), and (vi) cyclohexyl acetylene (system **6**). The reaction mechanism of systems **1−6** is studied in bulk solution and within (8,8) and (10,10) CNTs. The reaction mechanism is well-known, and in the absence of a metal catalyst, the formation of a triazole (P) occurs *via* a synchronous TS and after the two reactants interact in a RC. However, depending on how the two molecules are disposed spatially, the reaction can afford two possible regioisomers, i.e., the 1,4-triazole and the 1,5-triazole. In the absence of a metal catalyst, the reaction usually gives a mixture of both regioisomers without any selectivity.[88]

Figure 1 shows the two possible reaction pathways in the case of the reaction of benzyl azide with unsubstituted phenyl

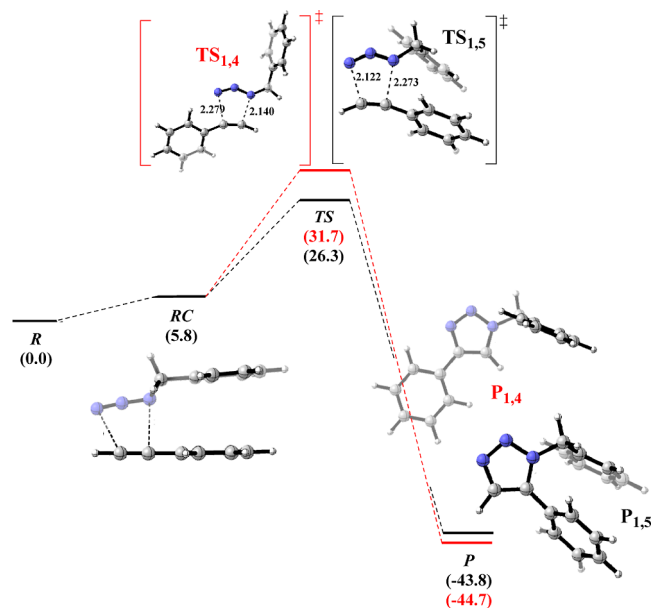**Figure 1.** Reaction profile with relative Gibbs energies (in kcal/mol) for the cycloaddition reaction between benzyl azide and phenylacetylene.

acetylene. As shown in Figure 1, both pathways share a common **RC** (ΔG = 5.8 kcal/mol), in which the phenyl ring of benzyl azide interacts only partially with the aromatic moiety of phenylacetylene since the methylene unity does not allow a good overlap between the two phenyl rings. At the same time, the N1−C5 distance is slightly shorter than the N3−C4 distance (3.450 Å for N1−C5 vs 3.492 Å for N3−C4), and thus N1 and C5 result more reactive with respect to other atoms. Following the pathway to form 1,5-triazole (1,5-pathway), the reactive system goes through **TS$_{1,5}$** ($\Delta G_{TS1,5}$ = 26.3 kcal/mol) where both the azide and the acetylene moiety bend to shorter N1−C5 and N3−C4 distances. Moreover, **TS$_{1,5}$** turns out to be asynchronous with the N3−C4 distance, much shorter than the N1−C5 distance (2.122 Å for the N3−C4 distance vs 2.273 Å for the N1−C5 distance). In contrast, following the other possible mechanism (1,4-pathway), the reactive system must overcome an overall activation energy barrier of 31.7 kcal/mol passing through **TS$_{1,4}$**. Like **TS$_{1,5}$**, **TS$_{1,4}$** is an asynchronous TS with N1−C5 distance shorter than the N3−C4 distance (2.140 Å vs 2.279 Å, respectively). However, since the partial interaction between the phenyl rings is lost, **TS$_{1,4}$** results are destabilized with respect to **TS$_{1,5}$**. Finally, after overcoming the corresponding energy barriers, the 1,4-triazole **P$_{1,4}$** ($\Delta G_{P1,4}$ = −44.7 kcal/mol) and the 1,5-

triazole $P_{1,5}$ ($\Delta G_{P1,5}$ = −43.8 kcal/mol) are formed. $P_{1,4}$ is thus slightly thermodynamically favored, while $P_{1,5}$ turns out to be the kinetic product. However, since the products are almost isoenergetic, a mixture of both regioisomers is formed. The reaction profile was then reassessed again, changing the phenyl acetylene hydrogen in the *para* position with electron-withdrawing (systems **1** and **2**) and electron-donating (EDG) (systems **4** and **5**) groups.[89−91] Last but not least, steric effects were evaluated by analyzing the reaction of benzyl azide with **6**.

In Table 1, the results are summarized. In terms of kinetics, each reaction of benzyl azide with the systems tested **1−6** was kinetically more favored than the reaction with phenyl acetylene.

Table 1. Gibbs Energy Barriers and Product Complex Stability in Benzene (in kcal/mol) for Systems 1−6

system	RC	$TS_{1,4}$	$TS_{1,5}$	$P_{1,4}$	$P_{1,5}$
1	3.4	25.1	23.8	−47.3	−44.7
2	5.2	28.1	25.6	−45.2	−43.5
3	5.8	31.7	26.3	−44.7	−43.8
4	4.7	28.3	25.9	−45.1	−44.1
5	4.0	27.7	25.2	−45.1	−44.6
6	5.2	29.2	27.6	−43.9	−44.3

In particular, the nitro group is the most stabilizing substituent in both pathways ($\Delta\Delta G^{\ddagger}$ = −6.6 kcal/mol for 1,4-pathway and $\Delta\Delta G^{\ddagger}$ = −2.5 kcal/mol for 1,5-pathway) but losing in terms of regioselectivity since the difference in energy between $TS_{1,4}$ and $TS_{1,5}$ is only 1.3 kcal/mol (5.4 kcal/mol with phenyl acetylene). On the other hand, with the other substituents, there are no major changes in the stabilization of the 1,4-pathway kinetics ($\Delta\Delta G^{\ddagger}$ = −3.6, −3.4, and −4.0 kcal/mol for systems **2**, **4**, and **5**, respectively) and the 1,5-pathway kinetics ($\Delta\Delta G^{\ddagger}$ = −0.7, −0.4, and −1.1 kcal/mol for systems **2**, **4**, and **5**, respectively). System **6**, the cyclohexyl acetylene, still kinetically favors the 1,5-pathway (27.6 kcal/mol for $TS_{1,5}$ vs 29.2 kcal/mol for $TS_{1,4}$). However, while $TS_{1,4}$ is stabilized by 2.5 kcal/mol with respect to the case of unsubstituted phenyl acetylene, $TS_{1,5}$ is destabilized by 1.3 kcal/mol due to the higher steric hindrance of the cyclohexyl and the loss of $\pi-\pi$ interactions between the phenyl rings. Thermodynamically, the situation is similar. The nitro group in system **1** leads to more stable products ($\Delta\Delta G_{P1,4}$ = −2.6 kcal/mol vs $\Delta\Delta G_{P1,5}$ = −0.9 kcal/mol) with the difference in stability between the two isomers ($\Delta\Delta G$ = −2.6 kcal/mol) increased with respect to the unsubstituted case ($\Delta\Delta G$ = −0.9 kcal/mol). A larger difference in stability can still be found with **2**, while with EDG groups, the same difference remains constant or decreases. Then, it is worth mentioning that in the case of cyclohexyl (system **6**), the triazole P1,5 results are slightly more stable.

Reactivity inside CNT (8,8). Once the substituent effects on the reactivity in benzene were analyzed, the same reactions with systems **1−6** were studied within a (8,8) CNT (see Scheme 2). Unlike the benzene-phase reaction, the reaction is a bit more complicated. The reaction still starts with the initial formation of a **RC**, but after overcoming the activation barrier through **TS**, the product complex **PC** is formed. Only after extraction from the nanotube can the triazole be isolated. Since inside the CNT, the phenyl rings can interact with the nanotube wall, two possible **RCs** are now possible, stabilized by $\pi-\pi$ interactions. In one of the **RCs**, the phenyl rings are on

the same side as in $TS_{1,5}$, and in the other one, the phenyls point in opposite directions as in $TS_{1,4}$. However, for allowing comparison with benzene-phase reactions, the activation energy barriers and the product complex stabilities were calculated taking as a reference the more stable among the two **RC** regioisomers. First, the effects of confinement on kinetics were analyzed, and in Table 2, the activation energy barriers

Table 2. Activation Energy Barriers (in kcal/mol) within (8,8) and (10,10) CNTs Compared to Activation Energy Barriers in Benzene Phase for Systems 1−6

system	$TS_{1,4}$ @(8,8)	$TS_{1,5}$ @(8,8)	$TS_{1,4}$ @(10,10)	$TS_{1,5}$ @(10,10)	$TS_{1,4}$	$TS_{1,5}$
1	23.6	25.4	27.5	39.8	25.1	23.8
2	23.1	23.8	32.1	53.2	28.1	25.6
3	22.6	24.7	29.0	37.6	31.7	26.3
4	21.9	24.0	33.9	46.5	28.3	25.9
5	22.8	23.6	27.1	49.8	27.7	25.2
6	20.1	48.6	27.1	27.6	29.2	27.6

$\Delta G^{\ddagger}_{1,4}$@(8,8) and $\Delta G^{\ddagger}_{1,5}$@(8,8) for both pathways within CNT and the ones $\Delta G^{\ddagger}_{1,4}$ and $\Delta G^{\ddagger}_{1,5}$ without CNT are reported. It is worth noting that the 1,4-pathway is kinetically favored over the 1,5-one for each system within a (8,8) CNT, which is opposite to what happens in the absence of CNT.

Considering only electronic effects, the largest energy differences between the two pathways are found with systems **1**, **3**, and **4** ($\Delta\Delta G^{\ddagger}$ = −1.8, −2.1, and −2.0 kcal/mol, respectively). Another difference is the fact that 1,4 and 1,5-pathways are destabilized with the nitro group as a substituent (system **1**) with respect to system **3** by 1.1 and 0.8 kcal/mol, respectively. On the other hand, it is with a methoxy group ($\Delta\Delta G^{\ddagger}_{1,4}$@(8,8) = −0.6 kcal/mol and $\Delta\Delta G^{\ddagger}_{1,5}$@(8,8) = −0.7 kcal/mol) that both pathways are more stabilized. Finally, in terms of kinetics, the greatest selectivity toward the 1,4-triazole is with cyclohexyl acetylene (system **6**). $\Delta G^{\ddagger}_{1,4}$@(8,8) is even 9.1 kcal/mol lower than $\Delta G^{\ddagger}_{1,4}$, while $\Delta G^{\ddagger}_{1,5}$@(8,8) is 28.5 kcal/mol higher in energy than $\Delta G^{\ddagger}_{1,5}$@(8,8) since the nanotube diameter is not long enough to allow the phenyl and the cyclohexyl to be positioned into a sandwich-like structure.

From a thermodynamic perspective, the product complexes $PC_{1,4}$@(8.8) result more stable than $PC_{1,5}$@(8.8). Except for cyclohexyl acetylene, the differences in stabilities between the complexes are in the range 6−9 kcal/mol. Once again, the nitro group is the substituent leading to the greatest difference in energies between $PC_{1,4}$@(8,8) and $PC_{1,5}$@(8,8) with the first one 8.7 kcal/mol more stable than the second one. In addition, bromo and amino groups have similar selectivities toward 1,4-regioisomer ($\Delta\Delta G$ = −7.7 and −7.5 kcal/mol, respectively), and the same applies when comparing phenyl and methoxy ($\Delta\Delta G$ = −5.9 and −6.1 kcal/mol, respectively).

Reactivity inside CNT (10,10). The 1,3-dipolar reaction was investigated also inside a (10,10) CNT (see Scheme 2), whose diameter is 13.57 Å. Thus, the molecules inside this larger tube suffer less steric hindrance with respect to (8,8) CNT. Like in the case of (8,8) CNT, two reactant complexes are possible, and as such, the activation barrier and product complex stabilities are calculated taking the more stable **RC** complex as a reference. Consequently, in Table 3, the activation energy barriers were also summarized, and, like for (8,8) CNT (Table 2), the 1,4-pathway results are much more favored for systems **1−5** since the $TS_{1,4}$-like **RC** results are

Table 3. Product Complex Stabilities (in kcal/mol) within (8,8) and (10,10) CNTs Compared to Product Stabilities in Benzene-Phase Reactions for Systems 1−6

system	$PC_{1,4}$ @(10,10)	$PC_{1,5}$ @(10,10)	$PC_{1,4}$ @(8,8)	$PC_{1,5}$ @(8,8)	$P_{1,4}$	$P_{1,5}$
1	−37.6	−29.8	−48.2	−39.5	−47.3	−44.7
2	−24.1	−16.2	−48.9	−41.2	−45.2	−43.5
3	−42.3	−32.5	−47.7	−41.8	−44.7	−43.8
4	−30.2	−23.5	−49.6	−43.5	−45.1	−44.1
5	−25.7	−19.8	−48.7	−41.2	−45.1	−44.6
6	−41.3	−40.6	−52.5	−22.0	−43.9	−44.3

more stabilized by the CNT than the $TS_{1,5}$-like **RC**. Furthermore, since the CNT diameter is large, the critical points cannot be fully stabilized by the interaction with the nanotube walls, and in addition, the systems are slightly deformed trying to fit the nonplanar nanotube wall. Therefore, the energy may result in an intermediate situation between a graphene phase and the reaction within the (8,8) CNT (see Table 4).

Table 4. EDA Analysis (in kcal/mol) between the Benzyl Azide and the Substituted Acetylene in the Benzene-Phase Reaction[a]

	ΔE_{strain}	ΔE_{int}	ΔV_{elstat}	ΔE_{Pauli}	ΔE_{oi}	ΔE_{disp}
			RC			
1	0.3	−10.2	−8.9	17.5	−3.3	−15.6
2	0.3	−9.7	−8.5	17.4	−3.3	−15.3
3	0.3	−8.1	−7.2	15.1	−2.9	−13.1
4	0.3	−9.1	−7.6	16.4	−3.2	−14.7
5	0.4	−9.0	−8.1	16.6	−3.3	−14.3
6	0.6	−8.1	−6.8	12.8	−3.0	−11.1
			$TS_{1,4}$			
1	22.7	−10.3	−43.8	86.7	−46.6	−6.6
2	23.8	−10.4	−40.6	78.8	−42.0	−6.7
3	23.9	−10.1	−40.3	78.6	−41.8	−6.6
4	24.2	−10.2	−40.1	77.9	−41.4	−6.6
5	24.2	−10.2	−39.9	77.3	−41.0	−6.6
6	24.6	−11.3	−41.2	79.3	−42.2	−7.2
			$TS_{1,5}$			
1	25.1	−17.4	−46.6	93.5	−47.2	−17.1
2	25.2	−16.7	−45.6	91.8	−45.7	−17.2
3	24.3	−14.7	−43.6	86.7	−44.5	−13.4
4	24.4	−14.6	−43.6	87.1	−44.5	−13.6
5	24.4	−14.6	−43.6	87.1	−44.4	−13.7
6	25.1	−14.4	−41.2	82.1	−42.6	−12.7

[a]Performed at the ZORA-BLYP-D3(BJ)/TZP level of theory in the gas phase on the equilibrium geometries in benzene.

For that reason, the activation energy barriers for the 1,4-path result resemble those of the benzene phase. Particularly, they are 2.4, 4.0, and 5.6 kcal/mol higher than the latter for systems **1**, **2**, and **4**, respectively, while for systems **3** and **5**, they are 2.7 and 0.6 kcal/mol lower, respectively. Finally, with the cyclohexyl group (system **6**), the $TS_{1,5}$-like results are slightly more stable than the other one, being $\Delta G^{\ddagger}_{1,4}$@(10,10) only 0.5 kcal/mol lower than $\Delta G^{\ddagger}_{1,5}$@(10,10) similarly to benzene-phase reactions. In addition, $\Delta G^{\ddagger}_{1,4}$@(10,10) results 2.1 kcal/mol lower than $\Delta G^{\ddagger}_{1,4}$, while $\Delta G^{\ddagger}_{1,4}$@(10,10) is equal to $\Delta G^{\ddagger}_{1,5}$. Like for kinetics, the thermodynamics (Table 3) are also influenced by (10,10) CNT in $PC_{1,4}$@(10,10),

which is more stable than $PC_{1,5}$@(10,10). At the same time, in all cases, the product complexes are less stable than the benzene-phase intermediates due to the nonplanarity of the CNT wall. In particular, in the case of **2**, **4**, and **5**, **PCs** result more unstable with energies around −30.0 kcal/mol, almost 20 kcal/mol above the case without CNT. In contrast, with cyclohexyl (system **6**), the thermodynamics are similar to those calculated in absence of confinement. In this case, $PC_{1,4}$@(10,10) is slightly more stable with respect to $PC_{1,5}$@(10,10), while without CNT, it is the opposite. However, in terms of magnitude order, there is no significant difference with or without CNT.

EDA of Benzene-Phase Reaction. By evaluating in Table 1, we now analyze the electronic (systems **1−5**) and steric factors (system **6**) of the reaction in benzene, i.e., in the absence of CNTs. In the RC, the phenyl ring of benzyl azide partially interacts with the aromatic moiety of phenylacetylene. Hence, the 1,5 triazole formation is kinetically favored being the positions 1 and 5 closer and prone to react, while the thermodynamic products are 1,4-triazole, except in the case of the cyclohexyl substituent. Analyzing the electronic effects, both the EDG and the electron-withdrawing groups (EWGs) decrease the kinetics of formation of two regioisomers with respect to the unsubstituted phenyl. On the other hand, with cyclohexyl instead of phenyl, the kinetics increase, being cyclohexyl sterically hindered.

With the aim of understanding the above trends, a Kohn−Sham molecular orbital analysis together with a quantitative energy decomposition (EDA) analysis has been performed. First, with respect to the interaction energy of RC, ΔE_{int} increases for both EDG and EWG compared to unsubstituted system **3**. The attractive electrostatic interaction is the main factor responsible for such an effect, together with the orbital interaction, although at a lower extent. Both more attractive ΔV_{elstat} and ΔE_{oi} compensate the increase of larger repulsive ΔE_{Pauli} due to the increase of steric repulsion with the substituent in the phenyl acetylene. The nature of the interaction between the latter and the benzyl azide in **RC** is mainly electrostatic. In contrast, the trends of $\Delta G_{TS1,4}$ cannot be explained by EDA in **$TS_{1,4}$**, as ΔE_{int} is kept almost constant with either EDG or EWGs. However, in case of 1,5-triazole formation, EWG and EDG affect the kinetics differently. So, whereas for EDG ΔE_{int} is kept constant, for EWG, ΔE_{int} increases due to more attractive ΔV_{elstat} and ΔE_{oi} and is supported by ΔE_{disp} too. Now, for both $TS_{1,4}$ and $TS_{1,5}$ the nature of the interaction is clearly covalent. For completeness, whereas in the **RC**, the deformation of the two reactants is very small (ΔE_{strain} = 0.3−0.6 kcal/mol), those in the TSs experience a larger deformation, somehow larger in the case of $TS_{1,5}$ (24.3−25.2 kcal/mol).

Once discussed the interaction of benzyl azide and the substituted acetylene in the benzene-phase reaction, we proceeded to analyze it when the reaction takes place inside the nanotube. Importantly, despite the confinement given by the CNT, either (8,8) or (10,10), in case of **RC**, the interaction energy decreases. Nonetheless, the trends are kept; i.e., ΔE_{int} increases with either EDG or EWGs (Tables 5 and S1). Importantly, we have also computed the interaction between the **RC** and CNT (8,8) by means of an EDA. The corresponding values correlate with the above interaction between the benzyl azide and substituted acetylene. For instance, ΔE_{int} increases from H to either EDG or EWG (Table S2). At difference, EDA values for both $TS_{1,4}$ and $TS_{1,5}$

Table 5. EDA Analysis in Gas Phase between the Benzyl Azide and the Substituted Acetylene inside CNT (10,10).[a]

	ΔE_{strain}	ΔE_{int}	ΔV_{elstat}	ΔE_{Pauli}	ΔE_{oi}	ΔE_{disp}
			RC			
1	0.4	−2.6	−2.2	4.4	−1.2	−3.6
2	0.4	−2.9	−3.0	4.3	−1.1	−3.2
3	0.3	−2.4	−2.4	3.9	−0.9	−3.0
4	0.4	−2.7	−2.1	4.3	−1.2	−3.6
5	1.1	−3.9	−2.8	5.8	−1.7	−5.2
6	0.9	−2.6	−1.4	3.3	−0.7	−3.7
			TS$_{1,4}$			
1	26.9	−10.6	−40.4	78.0	−41.5	−6.8
2	26.6	−11.1	−41.2	79.0	−42.3	−6.8
3	26.8	−10.7	−40.6	78.6	−41.9	−6.8
4	27.1	−11.0	−40.8	78.4	−41.8	−6.8
5	27.9	−10.8	−40.5	78.0	−41.5	−6.8
6	24.7	−10.8	−39.9	77.4	−41.6	−6.7
			TS$_{1,5}$			
1	26.1	−18.3	−41.5	83.2	−46.7	−8.2
2	26.1	−16.4	−41.2	82.9	−46.4	−8.2
3	26.0	−15.2	−40.7	82.2	−46.0	−8.1
4	26.2	−15.9	−41.0	82.7	−46.2	−8.2
5	26.0	−14.7	−40.4	82.0	−45.9	−8.1
6	25.5	−8.6	−40.7	81.5	−44.8	−10.2

[a]Performed at the ZORA-BLYP-D3(BJ)/TZP level of theory in the gas phase on the equilibrium geometries obtained inside the CNT (10,10) in benzene.

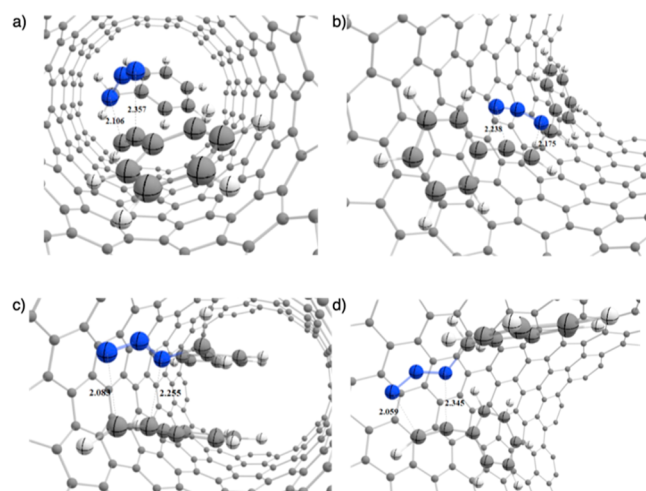are comparable to the nonconfined ones above. In this regard, Figure 2 includes how **TS$_{1,5}$** is tuned in the CNT (8,8) with

Figure 2. **TS$_{1,4}$** including substrate **3** in the (a) (8,8) and (b) (10.10) CNTs and **TS$_{1,5}$** including substrate **3** in the (c) (8,8) and (d) (10.10) CNTs (selected distances in Å.).

respect to the CNT (10,10). At first glance, the confinement favors both possible pathways by reducing the kinetic barriers except for the cyclohexyl substituent (**6**). In fact, while the 1,4-triazole pathway is favored by 9.1 kcal/mol, the 1,5-path results are kinetically forbidden ($\Delta\Delta G$ = +21.0 kcal/mol) due to high ΔE_{strain} and ΔE_{Pauli} (respectively, 31.27 and 119.90 kcal/mol vs the corresponding 28.71 and 102.87 kcal/mol when R is a phenyl, Tables 5 and S1) in **TS$_{1,5}$** structure. Focusing the analysis on the electronics, a stabilization by 2.3−8.1 kcal/mol was found regarding $\Delta G^{\ddagger}_{1,4}$, whereas $\Delta G^{\ddagger}_{1,5}$ is only slightly

stabilized ($\Delta\Delta G^{\ddagger} \approx 1.0–2.0$ kcal/mol) varying the substituents in the *para* position. The difference in stabilization between 1,4 and 1,5-pathways leads to a switch in the regioselectivity toward the 1,4-regioisomers. It is noteworthy that regioselectivity varies more with EDG than with EWG. Indeed, expressing the regioselectivity toward 1,4-pathway $S_{1,4}$ as the difference between $\Delta G^{\ddagger}_{1,4}$ and $\Delta G^{\ddagger}_{1,5}$, $S_{1,4}$ in a (8,8) nanotube is around 3 kcal/mol lower than in benzene when EWG is present, whereas in the presence of an EDG, $S_{1,4}$ is reduced by 4.5 kcal/mol within CNT. However, the major changes of $S_{1,4}$ occurs when no substituents are present ($\Delta S_{1,4}$ = −7.2) or the phenyl is substituted by a cyclohexyl ($\Delta S_{1,4}$ = −30.1). Finally, the performance of the reaction inside the nanotube drives to larger deformation energies, especially in the case of **TS$_{1,5}$** inside CNT (8,8), which is reduced with larger CNT (10,10).

To describe the importance of the steric effects, and taking into account past work related to the Tolman,[92] steric maps in Figure 3 were performed,[93,94] and the $\%V_{Bur}$[95] unveiled that
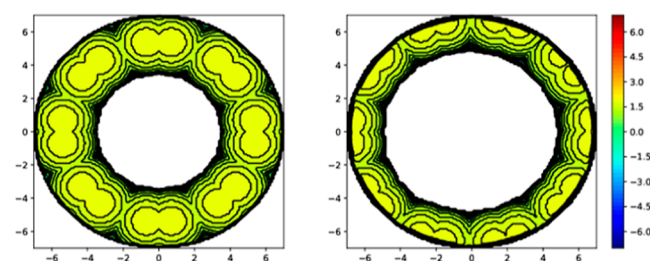

Figure 3. Steric maps of the *xy* plane, featuring the external ring, with a radius of 7.0 Å from the center of the ring, the length of the corresponding CNT on the *z* axis, and any of the carbon atoms providing the *xz* plane; curves are indicated in Å for CNT (8,8) on the left and (b) CNT (10,10) on the right (see Supporting Information for the steric maps with radii of 5.0, 6.0, and 10.0 Å).

there is a significant change from CNT (8,8) to CNT (10,10).[96−99] To confirm that the CNT does not hinder the reaction, we created steric maps to examine the cavity where reactivity occurs. The center point of the CNT section was used to define the *xy* plane, with the length along the *z*-axis. The diameters are 6.7 Å for CNT (8,8) and 9.5 Å for CNT (10,10). This analysis demonstrates that inserting the two substrates is less challenging for the narrower CNT. To further unveil the importance of the CNT, we studied the noncovalent interaction (NCI) in Figure 4 for transition states **TS$_{1,4}$** and **TS$_{1,5}$**. In these plots, green regions show attractive noncovalent interactions, whereas red regions refer to steric clashes. The NCI plots clearly show why **TS$_{1,5}$** is favored by both CNTs. At a particular level, in the case of CNT (8.8), the aryl groups of the two pieces of substrate make perfect $\pi–\pi$ stacking. This is evident in Figure 4a, both in the NCI 3D and in the 2D, where clearly in the favorable zone there is a thickening of the peaks.[100,101] In Figure 4b, on the other hand, it is observed how the force to stabilize the aryl groups with the nanotube gains with respect to each other, and thus both point toward the CNT (10,10), and therefore, the difference between **TS$_{1,4}$** and **TS$_{1,5}$** is much greater than for CNT (8,8), reaching 8.7 vs only 2.1 kcal/mol, according to Table 2. In general terms, CNT (8,8) improves the kinetics for **TS$_{1,4}$** always, whatever the substrate, with a range of 1.5−9.1 kcal/mol. This expresses that the CNT really favors the reaction. Moreover, how is it that the preference for the **TS$_{1,5}$** is lost despite $\pi–\pi$ stacking?
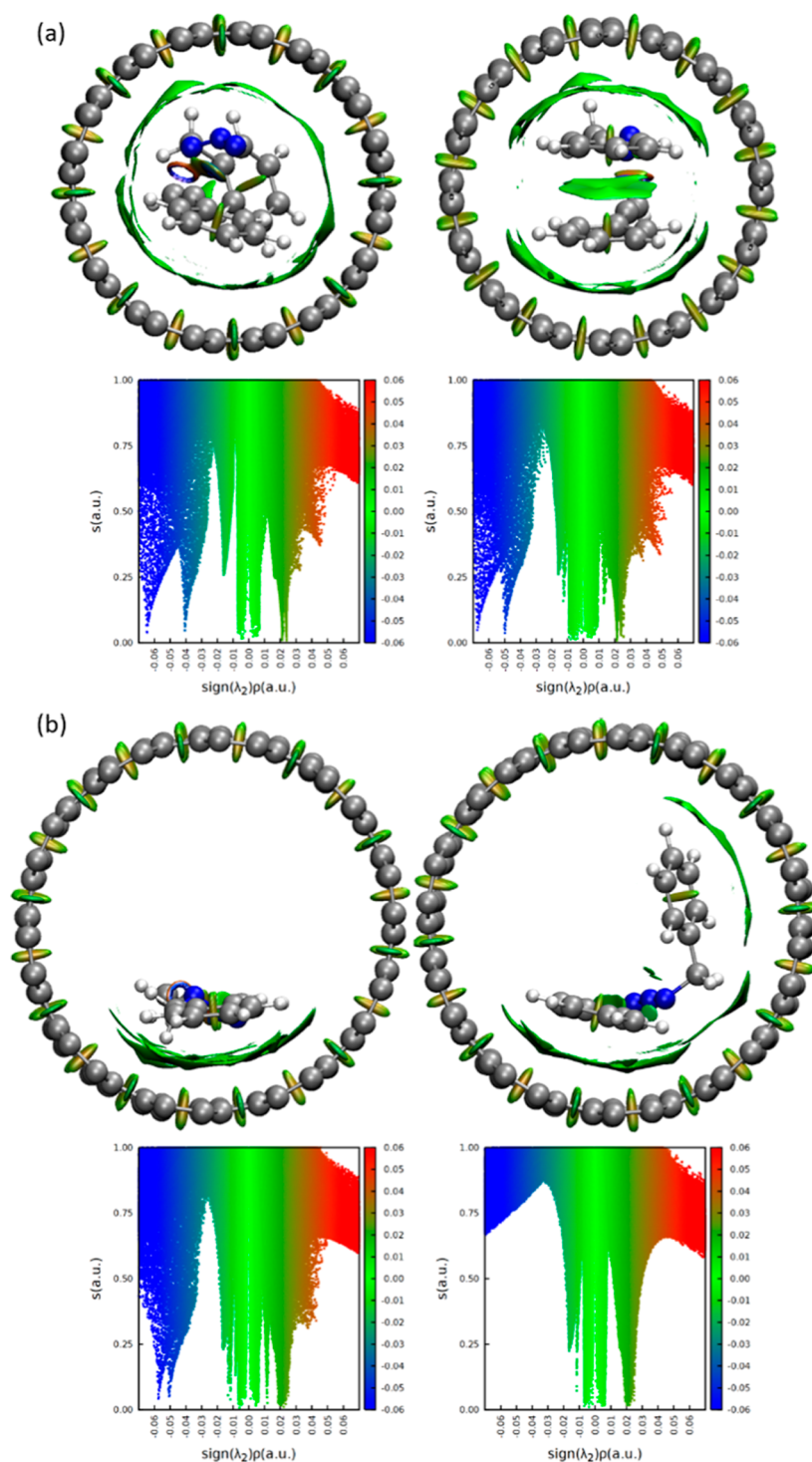
Figure 4. 2D and 3D NCI plots of the reduced density gradient (σ) vs sign (λ_2)ρ, in a.u. for **TS$_{1,4}$** (left) and **TS$_{1,5}$** (right) including substrate **3** for (a) CNT (8,8) and (b) CNT (10,10) (see Supporting Information for the 3D NCI plots with a perspective view). Green regions show attractive noncovalent interactions, whereas red ones show steric clashes.

So the answer is simple. The steric hindrance between the two substrates to interact with the walls of the CNT as a limiting agent does not give room. By extension, one would expect a better behavior for CNT (10,10) than for CNT (8,8), but it does not happen like this, as mentioned above. In fact, the corresponding kinetics worsens for **TS$_{1,4}$** by 2.4, 4.0, and 5.6 kcal/mol for systems **1**, **2**, and **4**, and improve to 2.7, 0.6, and 2.1 kcal/mol for systems **3**, **5**, and **6**, respectively. If we analyze the **TS$_{1,5}$**, in all cases, the CNT shows a worsening, and in a

very quantitative way, with an enormous range that goes from zero variability for the nonaryl alkyne **6** up to 27.6 kcal/mol for **2**. Going deeper, the energetic differences in the kinetics described in Table 2 exemplify that performing the reaction encapsulated in a CNT is kinetically disadvantaged by a CNT that cannot confront the aryl rings of the benzyl azide and the alkyne. In fact, if this last substrate does not have an aryl ring, as is the case for the alkyne system **6**, the barrier is shot for **TS$_{1,5}$** by CNT (8,8) up to 48.6 kcal/mol, compared to 27.6

kcal/mol without the CNT, and the NCI plots clearly confirm that the interaction with CNT is of a higher strength than between the two interacting units, and this was also evident in the above-arranged EDA results, confirming that a larger CNT diameter, if the substrates have aryl rings, hinders the reaction considered in this study.

CONCLUSIONS

The regioselectivity of the 1,3-dipolar cycloaddition reactions is significantly influenced by the confinement within CNTs. This computational study demonstrated that the regioselectivity shifts depending on whether the reaction occurs in the bulk phase (benzene) or inside CNTs. In the bulk phase, both regioisomers (1,4 and 1,5-triazoles) are formed with little selectivity, leading to a mixture of products. However, inside CNTs, the 1,4-pathway becomes kinetically favored due to spatial constraints and interactions with the nanotube walls. For reactions in benzene, the 1,5-pathway generally has a lower activation energy compared with the 1,4-pathway, making it the kinetically favored product. The thermodynamic products are nearly isoenergetic, resulting in a mixture of both regioisomers. Next, EWGs, partircularly the nitro group, increase the stability of the transition states and product complexes but reduce regioselectivity due to similar energy barriers for both pathways. EDGs show moderate effects on stability and selectivity. Next, substituents on the dipolarophiles significantly affect the reaction kinetics and thermodynamics, while EWG-substituted dipolarophiles stabilize the reaction intermediates and transition states more than EDG-substituted ones. In addition, cyclohexyl acetylene presents unique behavior due to steric hindrance, which influences both the reaction pathways and the stability of the resulting products.

Inside (8,8) CNTs, the 1,4-pathway is generally favored kinetically over the 1,5-pathway across all systems, contrary to the bulk phase. This is attributed to the $\pi-\pi$ interactions between the phenyl rings and CNT walls. In (10,10) CNTs, the difference in activation barriers between the two pathways is reduced, resembling more closely the behavior in the bulk phase, though the 1,4-pathway remains slightly favored.

EDA analyses revealed that the interaction energy in **RC** is mainly driven by electrostatic and orbital interactions. For TSs, covalent interactions dominate. In detail, the strain energy is minimal in the **RC** but increases significantly in the TS, particularly in the 1,5-pathway.

Overall, the study highlighted that confinement within CNTs not only alters the reaction pathways but also enhances the selectivity and stability of specific regioisomers. The findings suggest that CNTs can be effectively used to control and predict the outcomes of cycloaddition reactions, potentially leading to the selective synthesis of desired products in nanoconfined environments.

ASSOCIATED CONTENT

Ⓢ Supporting Information

The Supporting Information is available free of charge at https://pubs.acs.org/doi/10.1021/acs.jpcc.4c03830.

Details of the correlations and the EDA analyses (PDF)

Without CNT (XYZ)

CNT (8,8) (XYZ)

CNT (10,10) (XYZ)

AUTHOR INFORMATION

Corresponding Authors

Matteo Calveresi − *Università di Bologna, 40126 Bologna, Italy;* ⓞ orcid.org/0000-0002-9583-2146; Email: matteo.calvaresi3@unibo.it

Albert Poater − *Dipartimento di Chimica e Biologia, Università di Salerno, 84084 Fisciano, Italy;* ⓞ orcid.org/0000-0002-8997-2599; Email: albert.poater@udg.edu

Jordi Poater − *Departament de Química Inorgànica i Orgànica & IQTCUB, Universitat de Barcelona, 08028 Barcelona, Spain; ICREA, 08010 Barcelona, Spain;* ⓞ orcid.org/0000-0002-0814-5074; Email: jordi.poater@ub.edu

Authors

Michele Tomasini − *Institut de Química Computacional i Catàlisi, Departament de Química, Universitat de Girona, 17003 Girona, Catalonia, Spain; Dipartimento di Chimica e Biologia, Università di Salerno, 84084 Fisciano, Italy;* ⓞ orcid.org/0000-0002-1366-1401

Tainah Dorina Marforio − *Università di Bologna, 40126 Bologna, Italy;* ⓞ orcid.org/0000-0003-0690-306X

Complete contact information is available at:
https://pubs.acs.org/10.1021/acs.jpcc.4c03830

Notes

The authors declare no competing financial interest.

REFERENCES

(1) Noey, E. L.; Tibrewal, N.; Jiménez-Osés, G.; Osuna, S.; Park, J.; Bond, C. M.; Cascio, D.; Liang, J.; Zhang, X.; Huisman, G. W.; Tang, Y.; Houk, K. N. Origins of stereoselectivity in evolved ketoreductases. *Proc. Natl. Acad. Sci. U.S.A.* **2015**, *112*, E7065−E7072.

(2) Casadevall, G.; Duran, C.; Osuna, S. AlphaFold2 and Deep Learning for Elucidating Enzyme Conformational Flexibility and Its Application for Design. *JACS Au* **2023**, *3*, 1554−1562.

(3) Tanabe, K.; Holderich, W. F. Industrial applications of solid acid-base catalysts. *Appl. Catal., A* **1999**, *181*, 399−434.

(4) Smith, K.; El-Hiti, G. A. Use of zeolites for greener and more para-selective electrophilic aromatic substitution reactions. *Green Chem.* **2011**, *13*, 1579−1608.

(5) Breslow, R.; Dong, S. D. Biomimetic Reactions Catalyzed by Cyclodextrins and Their Derivatives. *Chem. Rev.* **1998**, *98*, 1997−2012.

(6) Chen, G.; Jiang, M. Cyclodextrin-based inclusion complexation bridging supramolecular chemistry and macromolecular self-assembly. *Chem. Soc. Rev.* **2011**, *40*, 2254−2266.

(7) Guo, D.-S.; Liu, Y. Calixarene-based supramolecular polymerization in solution. *Chem. Soc. Rev.* **2012**, *41*, 5907−5921.

(8) Mandolini, L.; Ungaro, R. *Calixarenes in Action;* Imperial College Press: London, U.K., 2000.

(9) Ramamurthy, V. Photochemistry within a water-soluble organic capsule. *Acc. Chem. Res.* **2015**, *48*, 2904−2917.

(10) Frischmann, P. D.; MacLachlan, M. J. Metallocavitands: an emerging class of functional multimetallic host molecules. *Chem. Soc. Rev.* **2013**, *42*, 871−890.

(11) Warmuth, R.; Yoon, J. Recent highlights in hemicarcerand chemistry. *Acc. Chem. Res.* **2001**, *34*, 95−105.

(12) Chernikova, E. Y.; Fedorov, Y. V.; Fedorova, O. A. Cucurbituril as a new "host" of organic molecules in inclusion complexes. *Russ. Chem. Bull.* **2012**, *61*, 1363−1390.

(13) Ni, X.-L.; Xiao, X.; Cong, H.; Liang, L.-L.; Cheng, K.; Cheng, X.-J.; Ji, N.-N.; Zhu, Q.-J.; Xue, S.-F.; Tao, Z. Cucurbit[*n*]uril based coordination chemistry: from simple coordination complexes to novel poly-dimensional coordination polymers. *Chem. Soc. Rev.* **2013**, *42*, 9480−9508.

(14) Guo, J.; Qin, Y.; Zhu, Y.; Zhang, X.; Long, C.; Zhao, M.; Tang, Z. Metal-organic frameworks as catalytic selectivity regulators for organic transformations. *Chem. Soc. Rev.* **2021**, *50*, 5366−5396.

(15) Hemmer, K.; Cokoja, M.; Fischer, R. A. Exploitation of Intrinsic Confinement Effects of MOFs in Catalysis. *ChemCatChem* **2021**, *13*, 1683−1691.

(16) Zarra, S.; Wood, D. M.; Roberts, D. A.; Nitschke, J. R. Molecular containers in complex chemical systems. *Chem. Soc. Rev.* **2015**, *44*, 419−432.

(17) Yoshizawa, M.; Klosterman, J. K.; Fujita, M. Functional molecular flasks: new properties and reactions within discrete, self-assembled hosts. *Angew. Chem., Int. Ed.* **2009**, *48*, 3418−3438.

(18) Dappe, Y. J. Encapsulation of organic molecules in carbon nanotubes: role of the van der Waals interactions. *J. Phys. D: Appl. Phys.* **2014**, *47*, 083001.

(19) Pop, E.; Mann, D.; Wang, Q.; Goodson, K.; Dai, H. Thermal conductance of an individual single-wall carbon nanotube above room temperature. *Nano Lett.* **2006**, *6*, 96−100.

(20) Yu, M.; Lourie, O.; Dyer, M. J.; Moloni, K.; Kelly, T. F.; Ruoff, R. S. Strength and breaking mechanism of multiwalled carbon nanotubes under tensile load. *Science* **2000**, *287*, 637−640.

(21) Dai, H. Carbon nanotubes: synthesis, integration and properties. *Acc. Chem. Res.* **2002**, *35*, 1035−1044.

(22) Khlobystov, A. N. Carbon nanotubes: from nano test tube to nano-reactor. *ACS Nano* **2011**, *5*, 9306−9312.

(23) Yumura, T.; Sugimori, N.; Fukuura, S. Theoretical understanding of stability of mechanically interlocked carbon nanotubes and their precursors. *Phys. Chem. Chem. Phys.* **2023**, *25*, 7527−7539.

(24) Chen, G.; Seki, Y.; Kimura, H.; Sakurai, S.; Yumura, M.; Hata, K.; Futaba, D. N. Diameter control of single-walled carbon nanotube forests from 1.3−3.0 nm by arc plasma deposition. *Sci. Rep.* **2014**, *4*, 3804.

(25) Poater, A.; Gallegos, A.; Carbó-Dorca, R.; Poater, J.; Solà, M.; Cavallo, L.; Worth, A. P. Modelling the structure-property relationships of nanoneedles: a journey towards nanomedicine. *J. Comput. Chem.* **2009**, *30*, 275−284.

(26) Cadena, A.; Botka, B.; Kamarás, K. Organic Molecules Encapsulated in Single-Walled Carbon Nanotubes. *Oxf. Open Mater. Sci.* **2021**, *1* (1), itab009.

(27) Fukuura, S.; Nishidate, Y.; Yumura, T. Performance of Particle Swarm Optimization in Predicting the Orientation of π-Conjugated Molecules Inside Carbon Nanotubes Compared with Density Functional Theory Calculations. *J. Phys. Chem. A* **2024**, *128*, 5054−5064.

(28) Marforio, T. D.; Tomasini, M.; Bottoni, A.; Zerbetto, F.; Mattioli, E. J.; Calvaresi, M. Deciphering the Reactive Pathways of Competitive Reactions inside Carbon Nanotubes. *Nanomater* **2023**, *13*, 8.

(29) Britz, D. A.; Khlobystov, A. N.; Porfyrakis, K.; Ardavan, A.; Briggs, G. A. D. Chemical reactions inside single-walled carbon nano test-tubes. *Chem. Commun.* **2005**, 37−39.

(30) Pagona, G.; Rotas, G.; Khlobystov, A. N.; Chamberlain, T. W.; Porfyrakis, K.; Tagmatarchis, N. Azafullerenes encapsulated within single-walled carbon nanotubes. *J. Am. Chem. Soc.* **2008**, *130*, 6062−6063.

(31) Pan, X.; Bao, X. The effects of confinement inside carbon nanotubes on catalysis. *Acc. Chem. Res.* **2011**, *44*, 553−562.

(32) Miners, S. A.; Rance, G. A.; Khlobystov, A. N. Chemical reactions confined within carbon nanotubes. *Chem. Soc. Rev.* **2016**, *45*, 4727−4746.

(33) Serp, P.; Castillejos, E. Catalysis in carbon nanotubes. *ChemCatChem* **2010**, *2*, 41−47.

(34) Allen, C. S.; Ito, Y.; Robertson, A. W.; Shinohara, H.; Warner, J. H. Two-dimensional coalescence dynamics of encapsulated metallofullerenes in carbon nanotubes. *ACS Nano* **2011**, *5*, 10084−10089.

(35) Talyzin, A. V.; Anoshkin, I. V.; Krasheninnikov, A. V.; Nieminen, R. M.; Nasibulin, A. G.; Jiang, H.; Kauppinen, E. I. Synthesis of graphene nanoribbons encapsulated in single-walled carbon nanotubes. *Nano Lett.* **2011**, *11*, 4352−4356.

(36) Chuvilin, A.; Bichoutskaia, E.; Gimenez-Lopez, M. C.; Chamberlain, T. W.; Rance, G. A.; Kuganathan, N.; Biskupek, J.; Kaiser, U.; Khlobystov, A. N. Self-assembly of a sulphur-terminated graphene nanoribbon within a single-walled carbon nanotube. *Nat. Mater.* **2011**, *10*, 687−692.

(37) Chernov, A. I.; Fedotov, P. V.; Talyzin, A. V.; Suarez Lopez, I.; Anoshkin, I. V.; Nasibulin, A. G.; Kauppinen, E. I.; Obraztsova, E. D. Optical properties of graphene nanoribbons encapsulated in single-walled carbon nanotubes. *ACS Nano* **2013**, *7*, 6346−6353.

(38) Botos, A.; Biskupek, J.; Chamberlain, T. W.; Rance, G. A.; Stoppiello, C. T.; Sloan, J.; Liu, Z.; Suenaga, K.; Kaiser, U.; Khlobystov, A. N. Carbon nanotubes as electrically active nanoreactors for multi-step inorganic synthesis: sequential transformations of molecules to nanoclusters and nanoclusters to nanoribbons. *J. Am. Chem. Soc.* **2016**, *138*, 8175−8183.

(39) Shiozawa, H.; Pichler, T.; Grüneis, A.; Pfeiffer, R.; Kuzmany, H.; Liu, Z.; Suenaga, K.; Kataura, H. A catalytic reaction inside a single-walled carbon nanotube. *Adv. Mater.* **2008**, *20*, 1443−1449.

(40) Lim, H. E.; Miyata, Y.; Kitaura, R.; Nishimura, Y.; Nishimoto, Y.; Irle, S.; Warner, J. H.; Kataura, H.; Shinohara, H. Growth of carbon nanotubes via twisted graphene nanoribbons. *Nat. Commun.* **2013**, *4*, 2548.

(41) Nakanishi, Y.; Omachi, H.; Fokina, N. A.; Schreiner, P. R.; Kitaura, R.; Dahl, J. E. P.; Carlson, R. M. K.; Shinohara, H. Template Synthesis of Linear-Chain Nanodiamonds Inside Carbon Nanotubes from Bridgehead-Halogenated Diamantane Precursors. *Angew. Chem., Int. Ed.* **2015**, *54*, 10802−10806.

(42) Fu, C.; Oviedo, M. B.; Zhu, Y.; von Wald Cresce, A.; Xu, K.; Li, G.; Itkis, M. E.; Haddon, R. C.; Chi, M.; Han, Y.; Wong, B. M.; Guo, J.; Guo, J. Confined Lithium-Sulfur Reactions in Narrow-Diameter Carbon Nanotubes Reveal Enhanced Electrochemical Reactivity. *ACS Nano* **2018**, *12*, 9775−9784.

(43) Miners, S. A.; Fay, M. W.; Baldoni, M.; Besley, E.; Khlobystov, A. N.; Rance, G. A. Steric and Electronic Control of 1,3-Dipolar Cycloaddition Reactions in Carbon Nanotube Nanoreactors. *J. Phys. Chem. C* **2019**, *123*, 6294−6302.

(44) Huisgen, R. Kinetics and mechanism of 1,3-dipolar cycloadditions. *Angew. Chem., Int. Ed.* **1963**, *2*, 633−645.

(45) Rostovtsev, V. V.; Green, L. G.; Fokin, V. V.; Sharpless, K. B. A stepwise Huisgen cycloaddition process: copper(I)-catalyzed regioselective "ligation" of azides and terminal alkynes. *Angew. Chem., Int. Ed.* **2002**, *41*, 2596−2599.

(46) Yumura, T.; Kertesz, M.; Iijima, S. Confinement Effects on Site-Preferences for Cycloadditions into Carbon Nanotubes. *Chem. Phys. Lett.* **2007**, *444*, 155−160.

(47) Chiacchio, M. A.; Legnani, L. Density Functional Theory Calculations: A Useful Tool to Investigate Mechanisms of 1,3-Dipolar Cycloaddition Reactions. *Int. J. Mol. Sci.* **2024**, *25*, 1298.

(48) Miners, S. A.; Rance, G. A.; Khlobystov, A. N. Regioselective control of aromatic halogenation reactions in carbon nanotube nanoreactors. *Chem. Commun.* **2013**, *49*, 5586−5588.

(49) Shao, J.; Yuan, L.; Hu, X.; Wu, Y.; Zhang, Z. The effect of nano confinement on the C−H activation and its corresponding structure-activity relationship. *Sci. Rep.* **2014**, *4*, 7225.

(50) Yumura, T.; Miki, R.; Fukuura, S.; Yamamoto, W. Energetics of Hybrid Structures between Cycloparaphenylene and Carbon Nanotubes: A Dispersion-Corrected Density Functional Theory Study. *J. Phys. Chem. C* **2020**, *124*, 17836−17847.

(51) Yumura, T.; Fukuura, S.; Miki, R. Roles of Carbon Nanotube Confinement in Enhancing Second-Order Nonlinear Optical Properties of Triiodobenzene Aggregates. *J. Phys. Chem. C* **2022**, *126*, 365−377.

(52) Yumura, T.; Yamamoto, W. Importance of the Alignment of Polar π Conjugated Molecules inside Carbon Nanotubes in Determining Second-Order Non-Linear Optical Properties. *Phys. Chem. Chem. Phys.* **2017**, *19*, 24819−24828.

(53) Yumura, T.; Yamashita, H. Key Factors in Determining the Arrangement of π-Conjugated Oligomers inside Carbon Nanotubes. *Phys. Chem. Chem. Phys.* **2015**, *17*, 22668−22677.

(54) Yamashita, H.; Yumura, T. The Role of Weak Bonding in Determining the Structure of Thiophene Oligomers inside Carbon Nanotubes. *J. Phys. Chem. C* **2012**, *116*, 9681−9690.

(55) Yumura, T.; Kertesz, M.; Iijima, S. Local Modifications of Single-Wall Carbon Nanotubes Induced by Bond Formation with Encapsulated Fullerenes. *J. Phys. Chem. B* **2007**, *111*, 1099−1109.

(56) Yumura, T.; Yamamoto, W. Kinetic Control in the Alignment of Polar π-Conjugated Molecules inside Carbon Nanotubes. *J. Phys. Chem. C* **2018**, *122*, 18151−18160.

(57) Smith, N. M.; Swaminathan Iyer, K.; Corry, B. The confined space inside carbon nanotubes can dictate the stereo- and regioselectivity of Diels-Alder reactions. *Phys. Chem. Chem. Phys.* **2014**, *16*, 6986−6989.

(58) Halls, M. D.; Schlegel, H. B. Chemistry inside carbon nanotubes: the Menshutkin SN2 reaction. *J. Phys. Chem. B* **2002**, *106*, 1921−1925.

(59) Halls, M. D.; Raghavachari, K. Carbon Nanotube Inner Phase Chemistry: The Cl− Exchange SN2 Reaction. *Nano Lett.* **2005**, *5*, 1861−1866.

(60) Giacinto, P.; Bottoni, A.; Calvaresi, M.; Zerbetto, F. Cl$^{(−)}$ Exchange S_N2 Reaction inside Carbon Nanotubes: C−H⋯π and Cl⋯π Interactions Govern the Course of the Reaction. *J. Phys. Chem. C* **2014**, *118*, 5032−5040.

(61) Giacinto, P.; Zerbetto, F.; Bottoni, A.; Calvaresi, M. CNT confinement effects on the Menshutkin SN2 reaction: the role of nonbonded interactions. *J. Chem. Theory Comput.* **2016**, *12*, 4082−4092.

(62) Marforio, T. D.; Bottoni, A.; Giacinto, P.; Zerbetto, F.; Calvaresi, M. Aromatic bromination of N-phenylacetamide inside CNTs: are CNTs real nanoreactors controlling regioselectivity and kinetics? A QM/MM investigation. *J. Phys. Chem. C* **2017**, *121*, 27674−27682.

(63) Fukuura, S.; Yumura, T. Roles of Carbon Nanotube Confinement in Modulating Regioselectivity of 1,3-Dipolar Cyclo-additions. *J. Phys. Chem. A* **2023**, *127*, 6962−6973.

(64) Escayola, S.; Bahri-Laleh, N.; Poater, A. %V$_{Bur}$ index and steric maps: from predictive catalysis to machine learning. *Chem. Soc. Rev.* **2024**, *53*, 853−882.

(65) Monreal-Corona, R.; Pla-Quintana, A.; Poater, A. Predictive catalysis: a valuable step towards machine learning. *Trends Chem.* **2023**, *5*, 935−946.

(66) Frisch, M. J.; Trucks, G. W.; Schlegel, H. B.; Scuseria, G. E.; Robb, M. A.; Cheeseman, J. R.; Scalmani, G.; Barone, V.; Mennucci, B.; Petersson, G. A.; Nakatsuji, H.; Caricato, M.; Li, X.; Hratchian, H. P.; Izmaylov, A. F.; Bloino, J.; Zheng, G.; Sonnenberg, J. L.; Hada, M.; Ehara, M.; Toyota, K.; Fukuda, R.; Hasegawa, J.; Ishida, M.; Nakajima, T.; Honda, Y.; Kitao, O.; Nakai, H.; Vreven, T.; Montgomery, J. A., Jr.; Peralta, J. E.; Ogliaro, F.; Bearpark, M.; Heyd, J. J.; Brothers, E.; Kudin, K. N.; Staroverov, V. N.; Kobayashi, R.; Normand, J.; Raghavachari, K.; Rendell, A.; Burant, J. C.; Iyengar, S. S.; Tomasi, J.; Cossi, M.; Rega, N.; Millam, J. M.; Klene, M.; Knox, J. E.; Cross, J. B.; Bakken, V.; Adamo, C.; Jaramillo, J.; Gomperts, R.; Stratmann, R. E.; Yazyev, O.; Austin, A. J.; Cammi, R.; Pomelli, C.; Ochterski, J. W.; Martin, R. L.; Morokuma, K.; Zakrzewski, V. G.;

Voth, G. A.; Salvador, P.; Dannenberg, J. J.; Dapprich, S.; Daniels, A. D.; Farkas, Ö.; Foresman, J. B.; Ortiz, J. V.; Cioslowski, J.; Fox, D. J. *Gaussian 09*, Revision E.01; Gaussian, Inc: Wallingford CT, 2009.

(67) Becke, A. D. Density-functional thermochemistry. V. Systematic optimization of exchange-correlation functionals. *J. Chem. Phys.* **1997**, *107*, 8554−8560.

(68) Schmider, H. L.; Becke, A. D. Optimized density functionals from the extended G2 test set. *J. Chem. Phys.* **1998**, *108*, 9624−9631.

(69) Chai, J.-D.; Head-Gordon, M. Systematic optimization of long-range corrected hybrid density functionals. *J. Chem. Phys.* **2008**, *128*, 084106.

(70) Grimme, S.; Antony, J.; Ehrlich, S.; Krieg, H. A consistent and accurate ab initio parametrization of density functional dispersion correction (DFT-D) for the 94 elements H-Pu. *J. Chem. Phys.* **2010**, *132*, 154104.

(71) Ditchfield, R.; Hehre, W. J.; Pople, J. A. Self-Consistent Molecular-Orbital Methods. IX. An Extended Gaussian-Type Basis for Molecular-Orbital Studies of Organic Molecules. *J. Chem. Phys.* **1971**, *54*, 724−728.

(72) Raghavachari, K.; Binkley, J. S.; Seeger, R.; Pople, J. A. Self-Consistent Molecular Orbital Methods. 20. Basis set for correlated wave-functions. *J. Chem. Phys.* **1980**, *72*, 650−654.

(73) Maseras, F.; Morokuma, K. IMOMM: A new integrated *ab initio* + molecular mechanics geometry optimization scheme of equilibrium structures and transition states. *J. Comput. Chem.* **1995**, *16*, 1170−1179.

(74) Zhao, Y.; Truhlar, D. G. The M06 suite of density functionals for main group thermochemistry, thermochemical kinetics, non-covalent interactions, excited states, and transition elements: two new functionals and systematic testing of four M06-class functionals and 12 other functionals. *Theor. Chem. Acc.* **2008**, *120*, 215−241.

(75) Weigend, F.; Ahlrichs, R. Balanced basis sets of split valence, triple zeta valence and quadruple zeta valence quality for H to Rn: Design and assessment of accuracy. *Phys. Chem. Chem. Phys.* **2005**, *7*, 3297−3305.

(76) Tomasi, J.; Persico, M. Molecular interactions in solution: an overview of methods based on continuous distributions of the solvent. *Chem. Rev.* **1994**, *94*, 2027−2094.

(77) Barone, V.; Cossi, M. Quantum calculation of molecular energies and energy gradients in solution by a conductor solvent model. *J. Phys. Chem. A* **1998**, *102*, 1995−2001.

(78) Cossi, M.; Rega, N.; Scalmani, G.; Barone, V. Energies, structures, and electronic properties of molecules in solution with the C-PCM solvation model. *J. Comput. Chem.* **2003**, *24*, 669−681.

(79) Grossman, E. F.; Daramola, D. A.; Botte, G. G. Comparing B3LYP and B97 Dispersion-corrected Functionals for Studying Adsorption and Vibrational Spectra in Nitrogen Reduction. *ChemistryOpen* **2021**, *10*, 316−326.

(80) Chopra, S. Performance study of the electronic and optical parameters of thermally activated delayed fluorescence nanosized emitters (CCX-I and CCX-II) via DFT, SCC-DFTB and B97−3c approaches. *J. Nanostruct. Chem.* **2020**, *10*, 115−124.

(81) Xu, Z.; Meher, B. R.; Eustache, D.; Wang, Y. Insight into the interaction between DNA bases and defective graphenes: Covalent or non-covalent. *J. Mol. Graphics Modell.* **2014**, *47*, 8−17.

(82) Aomchad, V.; Del Globo, S.; Poater, A.; D'Elia, V. Exploring the potential of Group III salen complexes for the conversion of CO_2 under ambient conditions. *Catal. Today* **2021**, *375*, 324−334.

(83) te Velde, G.; Bickelhaupt, F. M.; Baerends, E. J.; Fonseca Guerra, C.; van Gisbergen, S. J. A.; Snijders, J. G.; Ziegler, T. Chemistry with ADF. *J. Comput. Chem.* **2001**, *22*, 931−967.

(84) Becke, A. D. Density-functional exchange-energy approximation with correct asymptotic behavior. *Phys. Rev. A* **1988**, *38*, 3098−3100.

(85) Bickelhaupt, F. M.; Baerends, E. J. *Reviews in Computational Chemistry*; Lipkowitz, K. B., Boyd, D. B., Eds.; Wiley VCH: New York, 2000; Vol. *15*, pp 1−86.

(86) Fonseca Guerra, C.; Handgraaf, J.-W.; Baerends, E. J.; Bickelhaupt, F. M. Voronoi deformation density (VDD) charges:

Assessment of the Mulliken, Bader, Hirshfeld, Weinhold, and VDD methods for charge analysis. *J. Comput. Chem.* **2004**, *25*, 189−210.

(87) Nieuwland, C.; Vermeeren, P.; Bickelhaupt, F. M.; Fonseca Guerra, C. Understanding chemistry with the symmetry-decomposed Voronoi deformation density charge analysis. *J. Comput. Chem.* **2023**, *44*, 2108−2119.

(88) Chen, J.; Rebek, J. Selectivity in an Encapsulated Cycloaddition Reaction. *Org. Lett.* **2002**, *4*, 327−329.

(89) Hammett, L. P. The effect of structure upon the reactions of organic compounds, Benzene derivatives. *J. Am. Chem. Soc.* **1937**, *59*, 96−103.

(90) Yumura, T.; Yamashita, H. Modulating the Electronic Properties of Multimeric Thiophene Oligomers by Utilizing Carbon Nanotube Confinement. *J. Phys. Chem. C* **2014**, *118*, 5510−5522.

(91) Rao, C. N. R.; Voggu, R. Charge transfer with graphene and nanotubes. *Mater. Today* **2010**, *13*, 34−40.

(92) Tolman, C. A. Steric effects of phosphorus ligands in organometallic chemistry and homogeneous catalysis. *Chem. Rev.* **1977**, *77*, 313−348.

(93) Falivene, L.; Credendino, R.; Poater, A.; Petta, A.; Serra, L.; Oliva, R.; Scarano, V.; Cavallo, L. SambVca 2. A Web Tool for Analyzing Catalytic Pockets with Topographic Steric Maps. *Organometallics* **2016**, *35*, 2286−2293.

(94) Falivene, L.; Cao, Z.; Petta, A.; Serra, L.; Poater, A.; Oliva, R.; Scarano, V.; Cavallo, L. Towards the online computer-aided design of catalytic pockets. *Nat. Chem.* **2019**, *11*, 872−879.

(95) Poater, A.; Cosenza, B.; Correa, A.; Giudice, S.; Ragone, F.; Scarano, V.; Cavallo, L. Samb*V*ca: A Web Application for the Calculation of the Buried Volume of N-Heterocyclic Carbene Ligands. *Eur. J. Inorg. Chem.* **2009**, *2009*, 1759−1766.

(96) Bosson, J.; Poater, A.; Cavallo, L.; Nolan, S. P. Mechanism of Racemization of Chiral Alcohols Mediated by 16-Electron Ruthenium Complexes. *J. Am. Chem. Soc.* **2010**, *132*, 13146−13149.

(97) Poater, A.; Falivene, L.; Urbina-Blanco, C. A.; Manzini, S.; Nolan, S. P.; Cavallo, L. How does the addition of steric hindrance to a typical N-heterocyclic carbene ligand affect catalytic activity in olefin metathesis? *Dalton Trans.* **2013**, *42*, 7433−7439.

(98) Poater, A. Michael Acceptors Tuned by the Pivotal Aromaticity of Histidine to Block COVID-19 Activity. *J. Phys. Chem. Lett.* **2020**, *11*, 6262−6265.

(99) Arayachukiat, S.; Yingcharoen, P.; Vummaleti, S. V. C.; Cavallo, L.; Poater, A.; D'Elia, V. Cycloaddition of CO_2 to challenging N-tosyl aziridines using a halogen-free niobium complex: Catalytic activity and mechanistic insights. *Mol. Catal.* **2017**, *443*, 280−285.

(100) Poater, J.; Gimferrer, M.; Poater, A. Covalent and Ionic Capacity of MOFs To Sorb Small Gas Molecules. *Inorg. Chem.* **2018**, *57*, 6981−6990.

(101) Yousefi, S.; Bahri-Laleh, N.; Nekoomanesh, M.; Emami, M.; Sadjadi, S.; Amin Mirmohammadi, S.; Tomasini, M.; Bardají, E.; Poater, A. An efficient initiator system containing $AlCl_3$ and supported ionic-liquid for the synthesis of conventional grade polyisobutylene in mild conditions. *J. Mol. Liq.* **2022**, *367*, 120381.